HAL
open science

From crystalline to amorphous calcium pyrophosphates: a solid state Nuclear Magnetic Resonance perspective

Pierre Gras, Annabelle Baker, Christèle Combes, Christian Rey, Stéphanie Sarda, Adrian J. Wright, Mark E. Smith, John V. Hanna, Christel Gervais, Danielle Laurencin, et al.

To cite this version:

Pierre Gras, Annabelle Baker, Christèle Combes, Christian Rey, Stéphanie Sarda, et al.. From crystalline to amorphous calcium pyrophosphates: a solid state Nuclear Magnetic Resonance perspective. Acta Biomaterialia, 2016, 31, pp.348-357. 10.1016/j.actbio.2015.10.016 . hal-01221038

HAL Id: hal-01221038

https://hal.sorbonne-universite.fr/hal-01221038v1

Submitted on 27 Oct 2015

HAL is a multi-disciplinary open access archive for the deposit and dissemination of scientific research documents, whether they are published or not. The documents may come from teaching and research institutions in France or abroad, or from public or private research centers.

L'archive ouverte pluridisciplinaire **HAL**, est destinée au dépôt et à la diffusion de documents scientifiques de niveau recherche, publiés ou non, émanant des établissements d'enseignement et de recherche français ou étrangers, des laboratoires publics ou privés.

ACCEPTED MANUSCRIPT

From crystalline to amorphous calcium pyrophosphates: a solid state Nuclear Magnetic Resonance perspective

Pierre Gras[a], Annabelle Baker[b], Christèle Combes[a], Christian Rey[a], Stéphanie Sarda[c], Adrian J. Wright[b], Mark E. Smith[d,e], John V. Hanna[e], Christel Gervais[f], Danielle Laurencin[g] and Christian Bonhomme[f,]*

[a] CIRIMAT, INPT-CNRS-UPS, Université de Toulouse, ENSIACET, Toulouse, France

[b] School of Chemistry, University of Birmingham, Edgbaston, Birmingham, B15 2TT, UK

[c] CIRIMAT, INPT-CNRS-UPS, Université de Toulouse, Université Paul Sabatier, Toulouse, France

[d] Vice-Chancellor's Office, University House, Lancaster University, Lancaster, LA14YW, UK

[e] Department of Physics, University of Warwick, Coventry, CV4 7AL, UK UK

[f] Sorbonne Universités, UPMC Univ Paris 06, CNRS, Collège de France, UMR 7574, Chimie de la Matière Condensée de Paris, 75005, Paris, France

[g] Institut Charles Gerhardt de Montpellier, UMR 5253, CNRS-UM-ENSCM, Université de Montpellier, Montpellier, France

* To whom correspondence should be addressed: christian.bonhomme@upmc.fr

Tel: +33 1 44 27 15 06 Fax: +33 1 44 27 15

ACCEPTED MANUSCRIPT

Abstract

Hydrated calcium pyrophosphates (CPP, $Ca_2P_2O_7 \cdot nH_2O$) are a fundamental family of materials among osteoarticular pathologic calcifications. In this contribution, a comprehensive multinuclear NMR (Nuclear Magnetic Resonance) study of four crystalline and two amorphous phases of this family is presented. ^{1}H, ^{31}P and ^{43}Ca MAS (Magic Angle Spinning) NMR spectra were recorded, leading to informative fingerprints characterizing each compound. In particular, different ^{1}H and ^{43}Ca solid state NMR signatures were observed for the amorphous phases, depending on the synthetic procedure used. The NMR parameters of the crystalline phases were determined using the GIPAW (Gauge Including Projected Augmented Wave) DFT approach, based on first-principles calculations. In some cases, relaxed structures were found to improve the agreement between experimental and calculated values, demonstrating the importance of proton positions and pyrophosphate local geometry in this particular NMR crystallography approach. Such calculations serve as a basis for the future *ab initio* modeling of the amorphous CPP phases.

Keywords

Crystalline calcium pyrophosphates, amorphous calcium pyrophosphates, ^{1}H, ^{31}P, ^{43}Ca solid state NMR, first principles GIPAW calculations.

ACCEPTED MANUSCRIPT

ACCEPTED MANUSCRIPT

1. Introduction

Crystalline calcium pyrophosphate dihydrates (CPPD, $Ca_2P_2O_7{\cdot}2H_2O$) are among the most common forms of pathologic articular minerals: their prevalence increases with age, impacting on 17.5% of the population after the age of 80.[1] Although often asymptomatic, they are frequently involved or associated with acute articular arthritis such as pseudogout, and, more rarely, with chronic polyarthritis and destructive arthropathy; current treatments are mainly directed at relieving the symptoms of joint inflammation but not at inhibiting calcium pyrophosphate (CPP) formation nor at dissolving these crystals.[2,3,4]

CPP have been identified *in vivo* as two polymorphs of CPPD:[5] a triclinic form with a known structure,[6] and a monoclinic form with a recently solved structure[7] (respectively denoted as t-CPPD and m-CPPD). Other crystalline forms of hydrated calcium pyrophosphates have been synthesized *in vitro* and characterized, including a dimorphic monoclinic tetrahydrate (CPPT: $Ca_2P_2O_7{\cdot}4H_2O$), referred to as m-CPPT α and m-CPPT β.[8,9] Recently, Gras *et al.*[7] performed a systematic investigation of the synthesis of pure hydrated calcium pyrophosphates. They described the pH and temperature conditions leading to the formation of m-CPPT β, t-CPPD and m-CPPD,[10] as well as the identification of a new monohydrated calcium pyrophosphate phase exhibiting monoclinic symmetry, referred to as m-CPPM (CPPM: $Ca_2P_2O_7{\cdot}H_2O$),[11] and an unreferenced highly metastable trihydrated monoclinic calcium pyrophosphate phase derived from the structure of m-CPPT β.[12] The preparation of amorphous phases of biological interest, noted a-CPP ($Ca_2P_2O_7{\cdot}nH_2O$), has also been reported by Slater *et al.*[13] and Gras *et al.*,[10] and it was found that these phases are particularly stable compared to amorphous calcium orthophosphate and amorphous calcium carbonate.

ACCEPTED MANUSCRIPT

Several characterizations have been performed on all the hydrated calcium pyrophosphate phases mentioned above by several approaches, including powder XRD (X Ray diffraction) and vibrational spectroscopies, providing information on the configuration of the pyrophosphate groups.[10] It was observed that pyrophosphate ions in CPP phases have a wide range of P-O-P angles (between 123.1 and 134.1°).[8,9] This angle is important in understanding the relationship between the various CPP forms and their stability and transformation ability. Developing complementary tools for the characterization of hydrated calcium pyrophosphates is of particular interest, especially to understand the structure of phases like m-CPPD, for which the positioning of protons may be very difficult based exclusively on X-ray powder diffraction data, particularly considering that single crystals suitable for diffraction structure resolution are not yet available. Indeed, this phase has the highest inflammatory potential of all CPP phases, and it would be of interest to determine its structure in detail in order to understand the inflammation mechanism, which is possibly based on rupture of lysosome phospholipid membranes induced by pyrophosphate groups on the surface of the crystals.[14,15,16,17]

Solid state NMR is a technique which is attracting increasing attention for the study of synthetic and natural biomaterials[18] including calcium phosphate phases.[19,20,21,22,23,24,25,26,27] Indeed, solid state NMR can provide detailed atomic-scale information on the local structure around nuclei like ^{31}P, even in disordered and amorphous phases, and is therefore highly complementary to other analytical tools like XRD and IR (Infra Red) or Raman spectroscopies. NMR studies of calcium pyrophosphate phases have been very limited to date. To the best of our knowledge, ^{31}P NMR has only been applied to the characterization of the crystalline α- and β-$Ca_2P_2O_7$ anhydrous phases, and of a hydrated amorphous calcium pyrophosphate of composition ~ $Ca_2P_2O_7 \cdot 4H_2O$[13,28] In the latter case, the hydrolysis of the P-O-P bridge upon heat treatment was demonstrated using ^{1}H MAS, ^{31}P MAS and ^{1}H-^{31}P

ACCEPTED MANUSCRIPT

cross-polarisation (CP) MAS NMR experiments. With regards to ^{43}Ca NMR, only the anhydrous α-$Ca_2P_2O_7$ phase has been analyzed to date,[29] showing that the two crystallographically-inequivalent Ca sites can be unambiguously resolved at 14.1 T. Although ^{43}Ca is a more challenging nucleus than ^{31}P,[30,31] given its quadrupolar nature,[32] low natural abundance (0.014 %) and small magnetic moment (leading it to be a member of the group of so-called low-γ nuclei),[33] recent studies have shown that it can be very sensitive to subtle changes in Ca local environments.[34,35,36] Finally, even more challenging isotopes like oxygen-17 which usually require isotopic enrichment have been completely neglected so far.

The purpose of this study is to demonstrate, using a combined experimental-computational approach, how solid state NMR can be used for the structural investigation of calcium pyrophosphate phases, whether hydrated or anhydrous, and whether crystalline or amorphous. For this purpose, the ^{31}P, ^{43}Ca and ^{1}H MAS NMR spectra of a series of crystalline CPP phases (m-CPPD, t-CPPD, m-CPPT β and m-CPPM) are first reported, followed by those of amorphous calcium pyrophosphates. Then, we report the results of first-principles calculations of the NMR parameters of the crystalline calcium pyrophosphate phases, which were carried out using the Gauge-Including Projector Augmented Wave (GIPAW) approach.[37,38] The comparison between experimental and calculated NMR parameters not only validates the structural models of each compound allowing the assignment of P and Ca sites in crystalline phases, but also helps determine what atomic-scale information can be determined by solid state NMR. Interpretations of the NMR spectra of amorphous calcium pyrophosphate are given, a phase that has recently been proposed as an interesting component of bone cements.[39]

2. Materials and methods

ACCEPTED MANUSCRIPT

2.1 Syntheses

Crystalline hydrated calcium pyrophosphates m-CPPD, t-CPPD and m-CPPT β were synthesized following the methods previously published by Gras *et al.*,[10] by double decomposition between a potassium pyrophosphate solution and a calcium nitrate solution mixed into a buffer solution at a controlled temperature. The crystalline m-CPPM phase was prepared starting from m-CPPT β crystals and heating them at 110°C for 30 min as previously reported by Gras *et al.*[12]

The amorphous calcium pyrophosphate phases, of general formula $Ca_2P_2O_7.xH_2O$ (with x ~ 4),[10,13] were prepared using two different synthetic procedures. According to Gras,[10] precipitation at a controlled temperature (25°C) and pH (5.8) was used (compound referred to as "sample A" thereafter). According to Slater *et al.*[13] a precipitation at room temperature without any specific control/monitoring of the pH was also performed (compound referred to as "sample B" thereafter). In the latter case, the amorphous phase was also heat treated to 140 and 220 °C, in view of further solid state NMR characterizations of the transformations under temperature.

2.2 Characterization

2.2.1 General characterization

XRD measurements were performed using a Seifert XRD-3000TT diffractometer with a Cu Kα radiation (Cu $K\alpha_1$ $\lambda = 1.54060$ Å and Cu $K\alpha_2$ $\lambda = 1.54443$ Å), and equipped with a graphite monochromator. The XRD patterns were obtained between 2 and 70° (2θ) with a step size of 0.02° and a scan step time of 16 s at 298 K. The corresponding XRD powder patterns can be found in supporting information (Figure S1). The other characterization performed on the crystalline and amorphous synthesized phases, using notably vibrational spectroscopies,

ACCEPTED MANUSCRIPT

can be found in previous publications.[10,13]

2.2.2 ^{31}P solid state NMR

All ^{31}P MAS NMR data were recorded at 14.1 T using a VNMRS-600 (600 MHz ^{1}H frequency) spectrometer operating at a ^{31}P Larmor frequency of 242.81 MHz, using a Varian 3.2 mm HXY T3 MAS probe. MAS frequencies ranging from ~ 2.8 to 10 kHz were used in order to extract the chemical shift anisotropy (CSA) parameters. Experiments were performed using a set of saturation ^{31}P pulses, followed by a delay of 128 s, and a 90° excitation pulse of 2.5 µs. Spinal-64 ^{1}H decoupling (100 kHz RF) was applied during acquisition.[40] A total of 4 transients were acquired for each spectrum. The ^{31}P chemical shifts were referenced to $Si_5O(PO_4)_6$ as a secondary reference (at -44.0 ppm with respect to an 85% H_3PO_4 solution).[41] Temperature regulation was used during the experiments, to ensure that the temperature inside the rotor was ~ 10 °C. Prior to all experiments, the magic angle was carefully set in order to obtain the best ^{31}P MAS resolution, avoiding the reintroduction of any CSA or dipolar interaction which would broaden the spectra.

2.2.3 ^{43}Ca solid state NMR

Natural abundance ^{43}Ca MAS NMR data were acquired at 14.1 and 20.0 T using Varian VNMR-600 (600 MHz ^{1}H frequency) and Bruker Avance III-850 (850 MHz ^{1}H frequency) spectrometers operating at ^{43}Ca Larmor frequencies of 40.37 and 57.22 MHz, respectively. All ^{43}Ca chemical shifts were referenced at 0 ppm to a 1 mol.L^{-1} aqueous solution of $CaCl_2$.[29,30]

ACCEPTED MANUSCRIPT

The 14.1 T experiments were performed using a Varian 7.5 mm HXY MAS probe enabling MAS frequencies of 5 to 6 kHz, and the temperature was regulated at ~ 12°C throughout each measurement. The Double Frequency Sweep (DFS)[42,43] signal-enhancement scheme was applied for sensitivity enhancement prior to a selective 3.2 μs 90° solid pulse for the central transition. DFS parameters were optimized using ^{43}Ca-enriched $CaHPO_4$, with a convergence sweep from 300 to 70 kHz (duration ~ 5.5 ms; RF ~ 8 kHz), leading to an enhancement factor of ~ 2. Only m-CPPT β was recorded using a 9.5 mm Varian HX (for reasons unrelated to the nature of the sample); the spinning rate was set to 4 kHz, and the acquisition parameters for the DFS and excitation pulses were optimized in a similar fashion as described above.

At 850 MHz, a low-γ 7 mm Bruker MAS probe was used, spinning at 5 kHz. A RAPT (rotor-assisted population transfer)[44] enhancement scheme was applied prior to a 1.7 μs 90° solid pulse selective for the central transition. The RAPT pulses were first optimized on ^{43}Ca-enriched $CaHPO_4$, with an offset of 150 kHz (RF ~ 9 kHz), leading to an enhancement factor of ~ 2.

Details of the recycle delays, number of transients acquired, and total experimental times needed for each sample at both fields can be found in Table S1 (in supplementary information).

2.2.4 ^{1}H solid state NMR

^{1}H NMR spectra were recorded on a Varian VNMRS 600 MHz (14.1 T) NMR spectrometer at frequency of 599.82 MHz, using a 3.2 mm Varian T3 HXY MAS probe. Windowed-DUMBO (Decoupling Using Mind-Boggling Optimization)[45,46,47] ^{1}H MAS

ACCEPTED MANUSCRIPT

experiments were carried out at a spinning speed of 10 kHz. A glycine sample was used for the optimization of the DUMBO experiment. The radio-frequency (RF) field strength was 100 kHz, the duration of one DUMBO element 34.4 μs, and the observation window 0.8 μs. 20 transients were acquired, with recycle delays ranging from 4 to 16 s (depending on the sample). The ^{1}H chemical shifts were referenced externally to adamantane, used as a secondary reference (at 1.8 ppm with respect to tetramethylsilane, TMS). Temperature regulation was used during the experiments, to ensure that the temperature inside the rotor was ~ 10° C.

2.3 Calculations of NMR parameters

The first principles calculations based on the GIPAW[48] method were performed within Kohn-Sham DFT (Density Functional Theory) using the QUANTUM-ESPRESSO code.[49] The crystalline structure is described as an infinite periodic system using periodic boundary conditions. The NMR calculations were performed as follows: for hydrated phases, proton positions geometry optimization was carried out, starting from the published experimental structures of t-CPPD[50], m-CPPT β[51] and m-CPPD,[7] allowing the positions of protons to relax using the VASP (Vienna Ab Initio Simulation Package) code.[52] In the case of m-CPPM,[12] all atomic positions were relaxed to obtain a better agreement with the experimental data (see later in the text). The ^{1}H-relaxed structures are named "Rel H" hereafter, and the fully relaxed structure of m-CPPM is referred to as "Rel tot". The α-$Ca_2P_2O_7$[53] structure was calculated without further relaxation. For NMR calculations, the PBE generalized gradient approximation[54] was used and the valence electrons were described by norm conserving pseudopotentials[55] in the Kleinman-Bylander form.[56]

ACCEPTED MANUSCRIPT

The wave functions were expanded on a plane wave basis set with a kinetic energy cut-off of 80 Ry. The integral over the first Brillouin zone was performed using a Monkhorst-Pack 2×2×2 k-point grid. The principal components V_{xx}, V_{yy}, and V_{zz} of the electric field gradient (EFG) tensor defined with $|V_{zz}| \geq |V_{xx}| \geq |V_{yy}|$ were obtained by diagonalisation of the tensor. The quadrupolar interaction was then characterized by the quadrupolar coupling constant C_Q and the asymmetry parameter η_Q, which are defined as $C_Q = eQV_{zz}/h$ and $\eta_Q = (V_{yy} - V_{xx})/V_{zz}$. Absolute shielding tensors were obtained. To fix the ^{43}Ca scale, the calculated δ_{iso} (isotropic chemical shift) for a series of reference compounds were compared to experimental values[29] so that the average sum of experimental and calculated shifts coincide. Moreover, it should be noted that for the $C_Q(^{43}Ca)$ calculation, an updated quadrupole moment of –44.4 mb was used, as recently recommended by Bryce *et al.*[57] In the case of ^{31}P and ^{1}H, external referencing with respect to crystalline berlinite[58] ($\delta_{iso} = -24.5$ ppm)[59] for ^{31}P and α-glycine for ^{1}H[60] was chosen. Diagonalization of the symmetrical part of the calculated chemical shift tensor provides its principal components σ_{11}, σ_{22}, σ_{33} from which the chemical shift components δ_{11}, δ_{22}, δ_{33} can be calculated. δ_{11}, δ_{22} and δ_{33} are defined such as $|\delta_{33} - \delta_{iso}| \geq |\delta_{11} - \delta_{iso}| \geq |\delta_{22} - \delta_{iso}|$, and $\delta_{iso} = 1/3(\delta_{11} + \delta_{22} + \delta_{33})$. The CSA parameters are defined by $\delta_{CSA} = \delta_{33} - \delta_{iso}$ (anisotropy) and $\eta_{CSA} = |(\delta_{22} - \delta_{11})/\delta_{CSA}|$ (asymmetry).

3. Results and discussion

3.1 ^{31}P MAS NMR

^{31}P MAS NMR spectroscopy is the most used NMR approach for the study of calcium phosphate and pyrophosphate phases, because phosphorus-31 is a highly sensitive NMR isotope (100% natural abundance, I = ½, high receptivity). In the particular case of hydrated

ACCEPTED MANUSCRIPT

calcium pyrophosphate phases, four NMR interactions have to be considered, namely the CSA, the heteronuclear ^{31}P-^{1}H and homonuclear ^{31}P-^{31}P dipolar interactions, and the $^{2}J_{P-P}$ coupling. Under fast MAS and ^{1}H decoupling, the corresponding anisotropies are averaged efficiently leading to the determination of $\delta_{iso}(^{31}P)$. Usually, the $^{2}J_{P-P}$ couplings are not detected directly, although they can be revealed and measured using 2D (two dimensional) MAS experiments.[26,61] The number of isotropic lines is thus directly related to the number of inequivalent P sites in the asymmetric unit of a given structure.

^{31}P MAS NMR spectra were recorded for m-CPPT β, m-CPPD, t-CPPD and m-CPPM and are shown in Figure 1 (fast and slow MAS NMR spectra). At slow spinning frequency, numerous spinning sidebands are observed: their simulation by a CSA model[62] leads to the determination of the CSA parameters δ_{CSA} and η_{CSA} (as defined in the Materials and Methods section). Here, it is explicitly assumed that residual ^{31}P-^{31}P homonuclear dipolar couplings can be safely ignored in the simulations as they are much smaller (in Hz) than CSA effects. All simulations of the ^{31}P MAS NMR spectra are presented in Figure S2. As expected from the crystal structures, two distinct ^{31}P resonances are observed for each compound. For all spectra, the relative intensity of the two resonances differs from the expected 1:1 ratio, because the measurements were performed only for the purpose of determining the ^{31}P NMR parameters δ_{iso}, δ_{CSA} and η_{CSA}, and thus in conditions which do not necessarily ensure full relaxation of the different ^{31}P resonances. The observed range for $\delta_{iso}(^{31}P)$ is ~ −12 to −5 ppm (average value ~ −7.7 ppm), in agreement with data already published in the literature.[13,28] Concerning δ_{CSA}, the observed range is ~ 59 to 86 ppm, and the average value for all sites is ~ 77 ppm. The average values of $\delta_{iso}(^{31}P)$ and δ_{CSA} are fully compatible with the data obtained for a-CPP. In the case of a-CPP (Figure 1), a minor resonance centered at ~ 0 ppm is observed. As suggested by Slater *et al.*,[13] such a contribution can be safely assigned to PO_4^{3-} or HPO_4^{2-} moieties, caused by the presence of traces of orthophosphates in the precursors

ACCEPTED MANUSCRIPT

used to prepare CPP phases, and/or resulting from the partial hydrolysis of pyrophosphates under ageing.[10,13] As a matter of fact, the relative intensity of this particular resonance was found to increase with time (see supporting information, Figure S3).

Studying calcium pyrophosphates represents a challenge in terms of first principles calculations of ^{31}P chemical shifts, as the experimental resonances are closely separated (~ 1 ppm in the case of t-CPPD, see Table 1). The accuracy of the GIPAW method applied to ^{31}P has been reviewed previously.[63] Generally, the precision of such calculations depends explicitly on the accuracy of the corresponding structural data (obtained mainly by means of X-ray and/or neutron diffraction),[38] which means that the NMR data can act as constraints for the further refinement of a crystallographic structure. In the case of α-$Ca_2P_2O_7$, t-CPPD and m-CPPT β, good agreement is obtained between the experimental and calculated values both in terms of $\delta_{iso}(^{31}P)$ and δ_{CSA}. We notice that the calculated isotropic value for P1 in m-CPPT β is underestimated. Nevertheless, P1 and P2 can unequivocally be assigned.

The case of m-CPPD is an interesting one as it demonstrates the importance of proton relaxation. Indeed, starting from the published structure,[10] the assignment of P1 and P2 is not straightforward, because when assigning the sites based on the relative values of $\delta_{iso}(^{31}P)$, there is a contradiction with the relative order of the δ_{CSA} values (and *vice versa*). In contrast, starting from the m-CPPD relaxed structure (Rel H in Table 1, see section 2.3), the relative orders of $\delta_{iso}(^{31}P)$ and δ_{CSA} are correctly described by the GIPAW calculations. This point emphasizes the crucial importance of the H positions in the starting structure, in agreement with recent studies in the literature.[38,64] Moreover, we note that for m-CPPD, both P sites have similar proximities to protons (~ 2.7 to 2.8 Å), meaning that cross-polarization experiments cannot be used to distinguish them based on differences of CP dipolar dynamics. Finally, in the case of m-CPPM, even after relaxation of all atomic positions, the agreement with the

ACCEPTED MANUSCRIPT

experimental values remains poor but nonetheless allows a relatively safe assignment of the P1 and P2 sites since the relative order of the $\delta_{iso}(^{31}P)$ and δ_{CSA} values is consistent.

The geometric parameters of pyrophosphate ions (especially the P-O-P angle) have been used to explain the spectroscopic characteristics of vibrational spectra and correlations between band frequencies and geometric parameters have been described.[65,66,67] Given the variety of geometries of the different pyrophosphate anions in the crystal structures investigated here (Figure 2), several tests were performed to evaluate the influence of these parameters on the $\delta_{iso}(^{31}P)$ and δ_{CSA}. Using the IVTON program,[68] geometric parameters were calculated, including P-O-P angles for the pyrophosphate units or, for each PO_4 tetrahedron, P-O distances, sphere radius, linear eccentricity, linear sphericity, volume distortion, volume eccentricity, volume sphericity, sphere volume, polyhedron volume, average bond distance, standard deviation of the bond distances, barycentre-centroid distance, difference in average distance centroid-barycentre, atom projection on barycentre-centroid vector and difference in average distance atom-centroid. No direct correlations were found between these geometric parameters and the $\delta_{iso}(^{31}P)$ or δ_{CSA} values (data not shown). The lack of correlation could be due to other effects related to the local environment of the pyrophosphates, including hydrogen bonding on pyrophosphate oxygen atoms. From an experimental perspective, ^{2}J(P-O-P) may also be more relevant parameters to determine,[61,63] as they might give additional insight on the P-O-P angles in each structure; however, these have not been measured to date.

The spectrum of a-CPP is characterized by a broadening of the unique resonance corresponding to a distribution of $\delta_{iso}(^{31}P)$. Such a distribution is related to variations of P-O bond lengths and P-O-P angles, and also to a distribution in the relative proximity of neighbouring Ca^{2+} cations and water molecules in these more disordered structures. Interestingly, the ^{31}P MAS NMR spectrum is not sensitive to the synthetic protocol used for the preparation of the amorphous phase (see Figure S4).

ACCEPTED MANUSCRIPT

3.2 ^{43}Ca MAS NMR

The natural abundance ^{43}Ca MAS NMR spectra of the crystalline phases were recorded at two different magnetic fields, in order to better constrain the quadrupolar parameters C_Q and η_Q extracted (Figures 3 and S5). Indeed, for ^{43}Ca, 1D experiments at a single magnetic field are generally insufficient to extract these parameters.[30] Moreover, given that high magnetic fields, large volume rotors and rather long experimental times (see Table S1) are usually essential for *natural abundance* ^{43}Ca MAS NMR, [29,30,35,36] the use of the 2D MQ (Multiple Quantum) MAS approaches can be excluded from a practical point of view.

As shown in Figure 3, the ^{43}Ca isotropic chemical shift is sensitive enough to readily distinguish the various CPP forms both in terms of $\delta_{iso}(^{43}Ca)$ and $C_Q(^{43}Ca)$. The ^{43}Ca MAS NMR spectra were fitted using pure second-order quadrupolar lineshapes[62] (see Table 2 and Figure S5). The spectra are clearly in agreement with the presence of two inequivalent Ca sites, Ca1 and Ca2, as observed in the corresponding crystallographic structures. For the different crystal structures obtained for the CPP phases, experimental $\delta_{iso}(^{43}Ca)$ were found to vary between ~ 7 and ~ 33 ppm, while experimental $C_Q(^{43}Ca)$ between ~ 1.8 and ~ 4.5 MHz.

As a first attempt to correlate ^{43}Ca NMR parameters to the local environment of calcium in these materials, the calculated $\delta_{iso}(^{43}Ca)$ was plotted as a function of the average Ca-O bond distance (see Figure 4 and Table S2). $\delta_{iso}(^{43}Ca)$ globally decreases as the average Ca-O bond distance increases, in agreement with the different trends reported so far for other inorganic compounds of different oxygen-bonded families.[29,30] Interestingly, by looking more specifically at the different Ca local environments in the structures and analyzing in more detail the nature and number of the oxygen-bonded ligands coordinated to Ca, a better analysis could be proposed. Indeed, depending on the structures, the Ca^{2+} can be between 6-

ACCEPTED MANUSCRIPT

and 8- coordinated, and the ligands can be either only O atoms belonging to pyrophosphates, or to water molecules. As shown in Figure 4, the nature of the oxygenated ligand (pyrophosphate or water) does not appear to have a big influence, but when separating the Ca sites according to their coordination number, different zones can be clearly distinguished, depending on whether the Ca is 6-, 7- or 8- coordinated. This shows that the two main parameters which appear to govern the $\delta_{iso}(^{43}Ca)$ in the case of calcium pyrophosphates are the *average Ca…O bond distance* and the *coordination number* around the Ca. Finally, we note that similar trends were also observed using experimental $\delta_{iso}(^{43}Ca)$ values, rather than the calculated ones.

The high sensitivity of $\delta_{iso}(^{43}Ca)$ towards its local environment shows that it is a highly relevant tool of investigation of the structure of a-CPP at the atomic scale. In Figure 5, the high field ^{43}Ca MAS NMR spectrum of an a-CPP phase is presented (sample B – see section 2.1). The rather symmetrical lineshape observed covers the range of all resonances observed for the crystalline CPP phases, and is more specifically centered around the resonances of m-CPPT β, in agreement with elemental analyses which suggests the presence of an average of 4 water molecules.[13] Nonetheless, at this stage, no chemical shift and/or quadrupolar distribution could be extracted for a-CPP.

High field ^{43}Ca NMR was actually found to be a highly relevant tool of analysis of other related a-CPP phases. Indeed, depending on the synthetic protocol (control or not of the pH during the precipitation of a-CPP), ^{43}Ca MAS NMR spectra presented subtle differences (see Figure S6 for the comparison of samples A and B), showing that the structures of these materials actually slightly differ, despite the similarities in the ^{31}P MAS NMR data (see Figure S4). Finally, it is worth noting that the effect of heat-treatment of a-CPP could also be followed by ^{43}Ca MAS NMR (Figure S7). Indeed, despite rather symmetrical lineshapes at 20.0 T, a broadening of the signal was clearly observed after having heated the a-CPP phase

ACCEPTED MANUSCRIPT

at 220 °C, indicating an increase of the distribution of the ^{43}Ca NMR parameters, possibly due to the formation of hydrogen-phosphate anions within the material, as previously evidenced by ^{1}H and ^{31}P MAS NMR.[13] All in all, ^{43}Ca NMR appears as a valuable tool for investigation of hydrated calcium pyrophosphates, which would deserve to be looked into more systematically, as it can provide complementary information about their structure at the atomic scale.

3.3 ^{1}H MAS NMR

Finally, ^{1}H MAS NMR spectra were recorded using homonuclear decoupling (DUMBO) during acquisition (Figure 6). Despite the use of advanced decoupling techniques, it was not possible to fully resolve the different ^{1}H resonances related to inequivalent water molecules in the structures. For all crystalline structures an average value of ~ 5-6 ppm was observed. Such a range of isotropic chemical shifts is compatible with those obtained for protons involved in H-bond networks.[19]

A comparison with GIPAW calculated ^{1}H chemical shifts (Table S3) is also presented in Figure 6 for t-CPPD, m-CPPD, m-CPPM and m-CPPT β. As already stated in the ^{31}P discussion, the scatter of the calculated values is more pronounced in the case of m-CPPD. This observation tends to suggest that it should be possible to improve the positioning of the protons in the structure using the ^{1}H chemical shifts as constraints.

The ^{1}H MAS spectra of a-CPP phases prepared according to different synthetic procedures were found to exhibit distinct signatures. While only one main asymmetric signal was observed for the sample prepared by simple precipitation (sample B), two distinct resonances were visible when the pH of the precipitating solution was controlled (sample A).

ACCEPTED MANUSCRIPT

This observation shows that differences in the atomic-scale structure of both amorphous compounds exist, as already suggested by ^{43}Ca MAS NMR. More specifically, the ^{1}H NMR spectrum of the a-CPP phase called sample B resembles that of m-CPPT β, while additional ^{1}H local environments are observed in sample A, which could be similar to those observed in m-CPPM, given the similarity in ^{1}H chemical shifts. Thus, it appears that despite the fact that the water content in both phases is very similar,[10,13] the H-bond network of the water molecules within these amorphous phases depends on the synthetic protocol. A more systematic investigation of the ^{1}H NMR spectra of amorphous calcium pyrophosphates precipitated at different pH values may therefore shed light on the structural variability of these materials at the atomic scale, by providing information which is not necessarily accessible from more commonly used techniques such as IR spectroscopy. Low temperature experiments (down to ~ 100 K) would also be of high interest for a more detailed comparison of experiment and GIPAW computed parameters. Indeed, water molecules must experience intrinsic dynamics in the various structures (at least at room temperature), as demonstrated by the relative lack of resolution of the ^{1}H MAS spectra. It follows that the ^{1}H isotropic chemical shifts observed at room temperature correspond to averages. Freezing local dynamics would lead to determine "static" isotropic chemical shifts which could be compared safely to GIPAW predictions and act therefore as pertinent constraints for structure refinement.

4. Conclusion

In this contribution, several hydrated calcium pyrophosphate phases (both crystalline and amorphous) were characterized by multinuclear MAS NMR. It was demonstrated that ^{31}P and ^{43}Ca MAS NMR spectroscopies are suitable for the clear distinction of the various phases. Even in the case of amorphous samples, subtle variations of the resonance lines were

ACCEPTED MANUSCRIPT

observed by ^{43}Ca MAS NMR depending on the synthetic protocol and heat treatment temperature. Moreover, ^{1}H NMR was found to be informative about differences in the H-bond networks within these phases.

All crystalline structures were then studied in the context of NMR crystallography, using GIPAW as a theoretical bridge between experimental and computed data. All in all, a fairly good agreement was observed for the three studied nuclei, provided that a relaxation of the structures (focusing especially on proton positions) was carried out. Nonetheless, discrepancies remained for the hydrated phases, which may be due to the fact that NMR calculations do not take into account any temperature/local motion effects. Previous studies have indeed shown that these factors could induce significant differences between experimental and computational data.[38]

Concerning a-CPP phases, important structural features have been derived from multinuclear solid state NMR analyses. First of all, the ^{31}P MAS spectra are rather insensitive to the synthetic protocols: it demonstrates that the ^{31}P NMR parameters are mostly determined by the local geometry of the $P_2O_7^{4-}$ species (angle, bond lengths) and not by the localization of the calcium cations and the water molecules. This is clearly not the case when considering ^{43}Ca and ^{1}H NMR parameters. In particular, ^{1}H MAS spectra seem suitable to distinguish local environments comparable to those observed in m-CPPT β and m-CPPM crystalline phases, though contents in water molecules are comparable from one sample to another one.

Slater *et al.*[13] already pointed out structural similarity between m-CPPT β and a-CPP by pair distribution functions (PDF) analysis. This structural similarity was furthermore linked to comparable behavior regarding hydrolysis reactions. Thus it has been observed that m-CPPT β, m-CPPM and a-CPP are hydrolyzed at high temperature but this is not the case for t-CPPD and m-CPPD samples.[10,12]

ACCEPTED MANUSCRIPT

Based on the elemental composition of the amorphous calcium pyrophosphate phases, and on the structural information gathered here by ^{1}H, ^{43}Ca and ^{31}P MAS NMR, realistic structural models for these amorphous phases are currently being developed. Following the pioneering approach initiated by Charpentier[37] and very recent results presented by the same author,[69] the idea is to compare the calculated NMR values for computational models of this material with the experimental ones, in order to propose a realistic model. This study will be presented in a forthcoming publication.

Finally, the contribution of this study in structural refinement of poorly known hydrated CPP phases is a first step towards the understanding of *in vivo* phenomena related to osteoarthritis: structure-inflammatory response relationships, potential precursor phase formation and evolution, role of trace elements in CPP crystal formation occurring in associated diseases like hypomagnesaemia,[70] Wilson's disease (copper excess)[71] and haemochromatosis (iron excess).[72] In addition, some applications of CPP compounds in the biomaterial field can be envisioned.[39]

5. Acknowledgements

The French/UK CNRS PICS project QMAT is acknowledged. D. Laurencin and M. E. Smith thank the Royal Society for funding collaborative research (Warwick-Montpellier JP090313 partnership). The UK 850 MHz solid-state NMR Facility used in this research was funded by EPSRC and BBSRC, as well as the University of Warwick including via part funding through Birmingham Science City Advanced Materials Projects 1 and 2 supported by Advantage West Midlands (AWM) and the European Regional Development Fund (ERDF). We thank Dr Dinu Iuga for his help at the 850 MHz Facility. NMR spectroscopic calculations were performed on the IDRIS supercomputer centre of the CNRS (Project: 091461). Finally, the authors thank the French Agence Nationale de la Recherche (CAPYROSIS project –

ACCEPTED MANUSCRIPT

ANR-12-BS08-0022-01) and the Institut National Polytechnique de Toulouse (PRECYPICA project – BQR INPT 2011) for supporting part of this research work.

ACCEPTED MANUSCRIPT

ACCEPTED MANUSCRIPT

Figure 1: ^{31}P MAS NMR spectra (decoupled from ^{1}H during the acquisition time) of t-CPPD, m-CPPD, m-CPPT β, m-CPPM and a-CPP (sample A) (14.1 T, 242.81 MHz, spinal 64 ^{1}H decoupling, relaxation delay: 128 s, number of scans: 4, regulation of the temperature: 10 °C, saturation pulses on the ^{31}P channel before the first 90° pulse). MAS rotation frequency: 10.0 kHz (left) and ~ 2.8 to 5.0 kHz (right). For the slow MAS spectra, the exact rotation frequency, ν_r, is specified in Figure S2 for each sample. For each spectrum, the arrow indicates the region of the isotropic resonances (two in general, except in the case of a-CPP). All other lines correspond to spinning sidebands from which CSA parameters can be extracted. In the case of a-CPP, the minor component at δ_{iso} ~ 0 ppm is assigned to orthophosphate species (see main text).

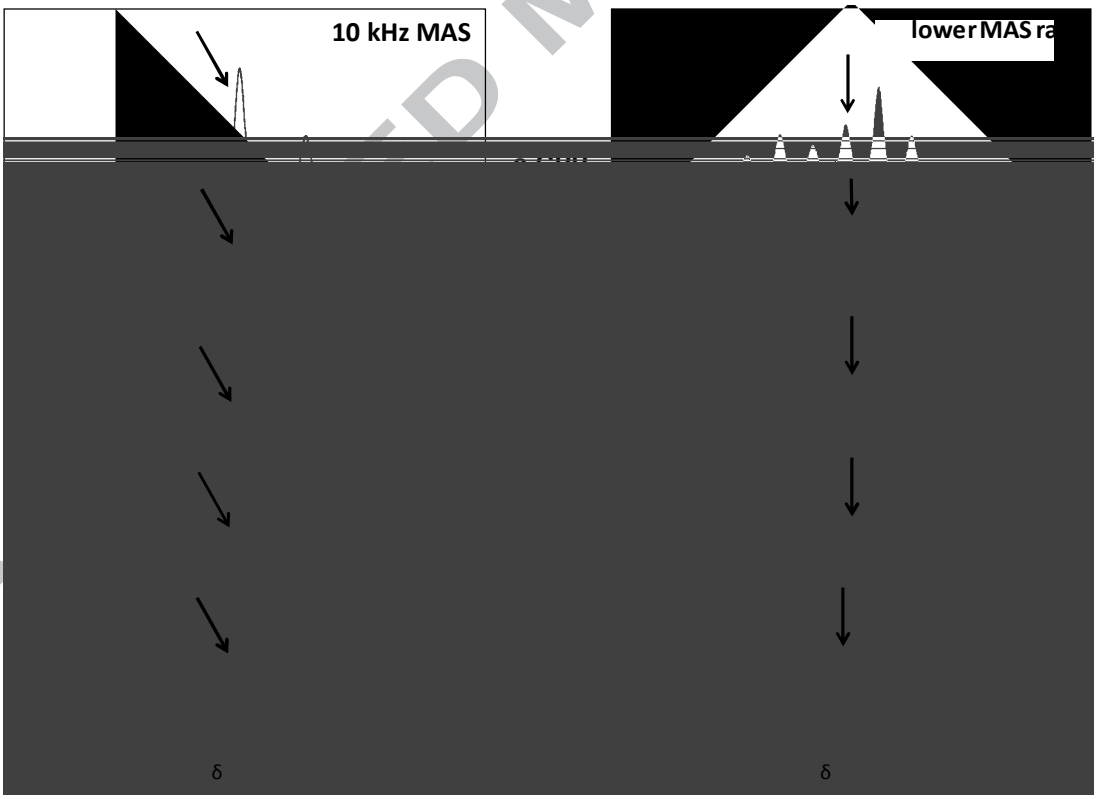

ACCEPTED MANUSCRIPT

Figure 2: Configuration of the pyrophosphate anions in the crystalline CPP phases studied (as shown along two different viewing directions). O and P atoms are in red and grey, respectively.

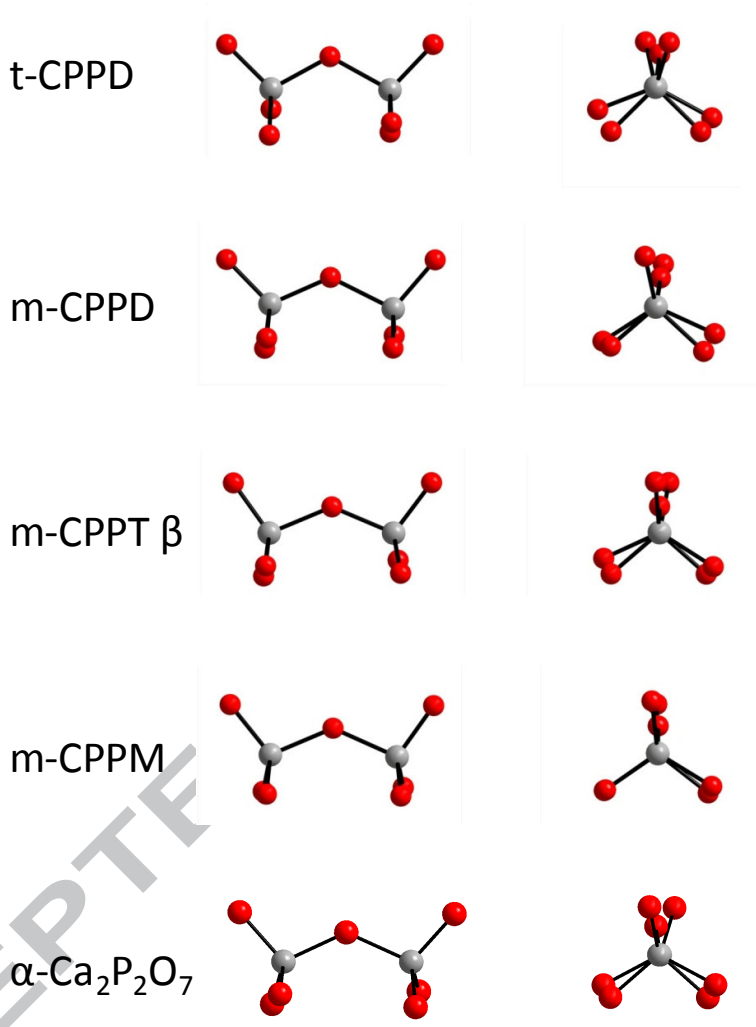

ACCEPTED MANUSCRIPT

ACCEPTED MANUSCRIPT

Figure 3: Natural abundance ^{43}Ca MAS NMR spectra of t-CPPD, m-CPPD, m-CPPT β and m-CPPM, recorded at 14.1 T [$\nu_0(^{43}Ca) = 40.37$ MHz], and 20.0 T [$\nu_0(^{43}Ca) = 57.22$ MHz]. MAS rotation frequency: between 4 and 6 kHz. For details on the relaxation delay and number of scans for each sample, see Table S1. The fitting of the different MAS NMR spectra can be found in Figure S5.

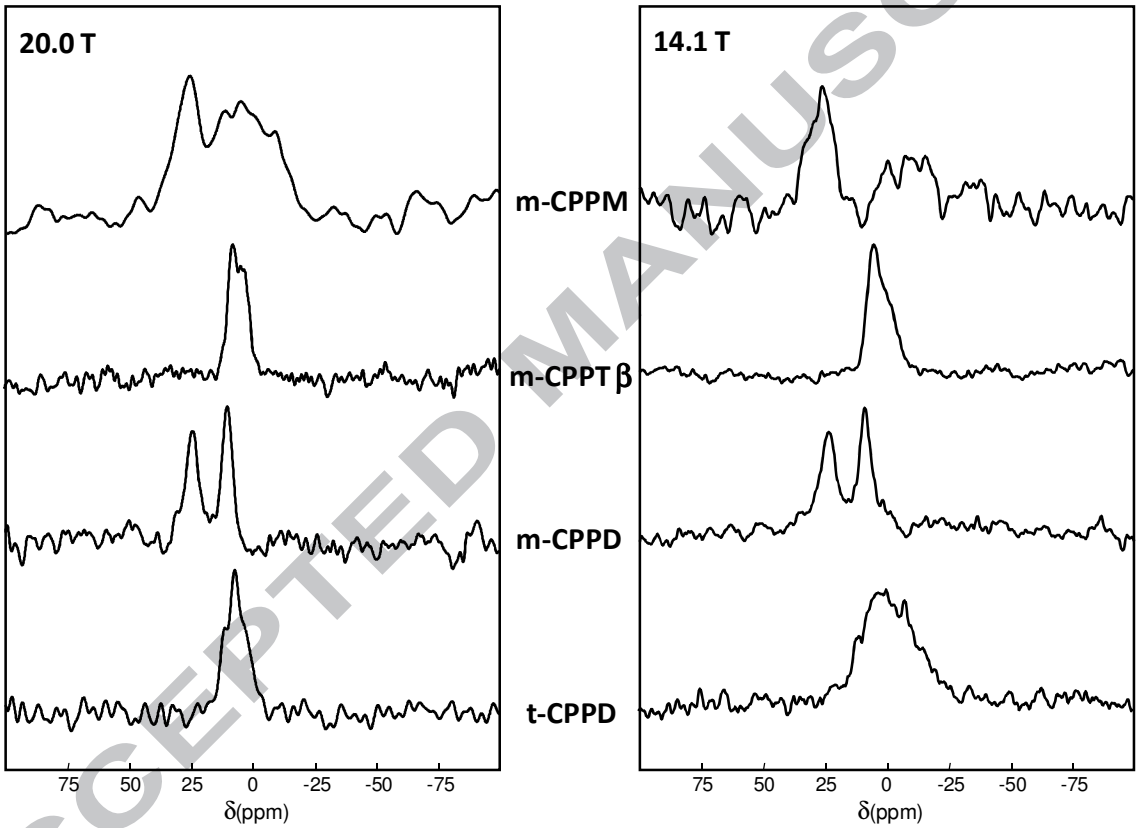

ACCEPTED MANUSCRIPT

ACCEPTED MANUSCRIPT

Figure 4: Correlation between the computed ^{43}Ca isotropic chemical shifts and the mean Ca…O bond distance in m-CPPD, t-CPPD, m-CPPT β, m-CPPM and α-$Ca_2P_2O_7$, depending on the Ca coordination number (CN) and the number of water molecules in the coordination sphere. The values are taken from Table S2.

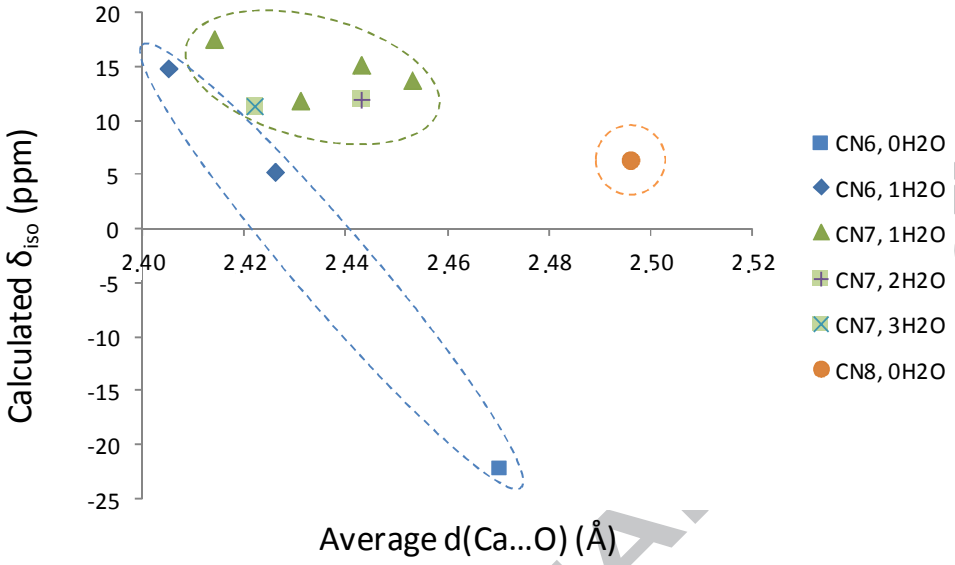

ACCEPTED MANUSCRIPT

ACCEPTED MANUSCRIPT

Figure 5: Natural abundance ^{43}Ca MAS NMR spectra of a-CPP (sample B – see section 2.1), t-CPPD, m-CPPD and m-CPPT β [20.0 T, $\nu_0(^{43}Ca)$ = 57.22 MHz; for relaxation delay and number of scans: see Table S1]. MAS rotation frequency: 5 kHz. Comparison between the ^{43}Ca MAS spectra of samples A and B are presented in Figure S6.

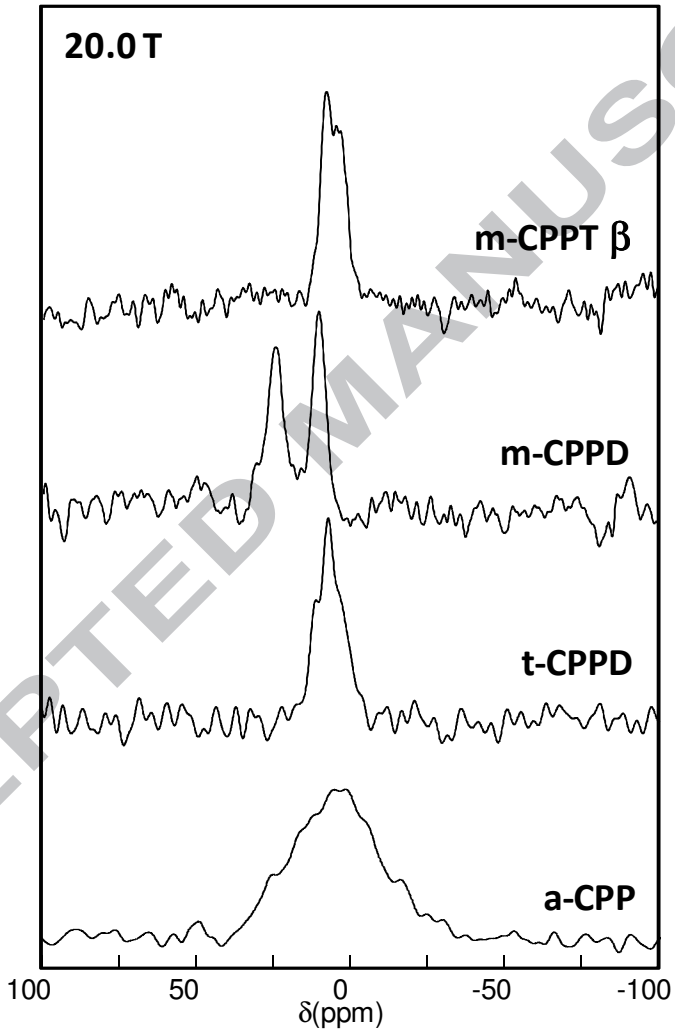

ACCEPTED MANUSCRIPT

ACCEPTED MANUSCRIPT

Figure 6: ^{1}H MAS NMR spectra of t-CPPD, m-CPPD, m-CPPT β, m-CPPM and a-CPP (samples A and B – see section 2.1) using windowed-DUMBO homonuclear decoupling during the acquisition (14.1 T, 599.82 MHz, relaxation delay: 4 to 16 s depending on the sample, number of scans: 20, regulation of the temperature: 10° C). MAS rotation frequency: 10.0 kHz. All observed resonances correspond to isotropic lines. In red: GIPAW calculations (see Table S3).

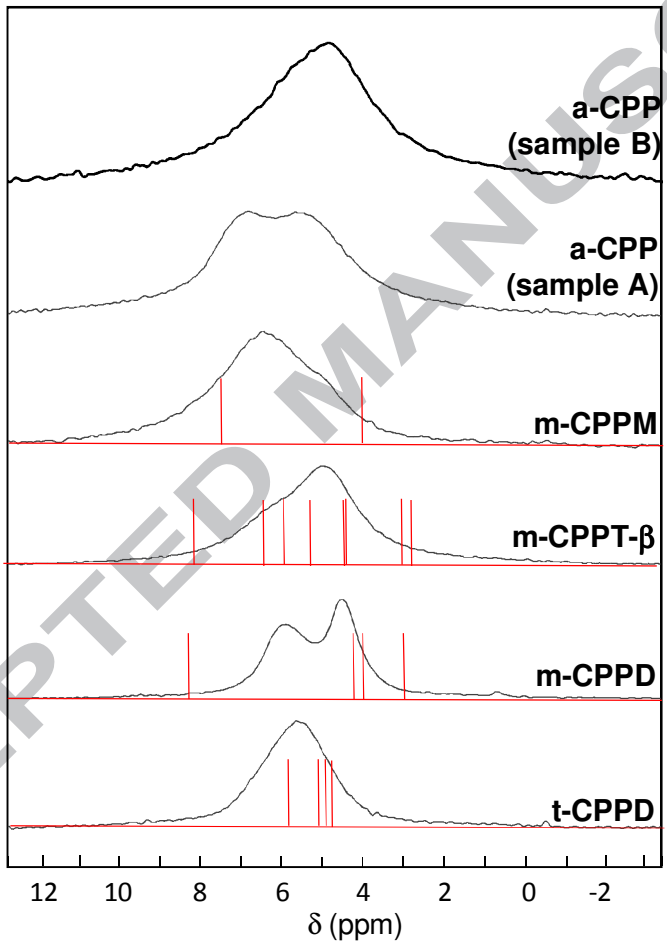

ACCEPTED MANUSCRIPT

ACCEPTED MANUSCRIPT

Table 1: Experimental and calculated ^{31}P chemical shift tensor (CSA) data for m-CPPD, m-CPPM, t-CPPD, m-CPPT β. The definitions of δ_{CSA} and η_{CSA} are given in the experimental section. In the case of m-CPPD, results obtained before and after relaxation of the proton positions ("Rel H") are presented. In order to validate the combined experimental/computational approach, both sets of data were added for α-$Ca_2P_2O_7$ (anhydrous phase). The maximum error on experimental δ_{iso} values was estimated to 0.15 ppm.

		δ_{iso} (ppm)		δ_{CSA} (ppm)		η_{CSA}	
		Exp	Calc	Exp	Calc	Exp	Calc
α-$Ca_2P_2O_7$	P1	−7.70	−9.38	59.4	65.58	0.62	0.53
	P2	−10.00	−10.39	66.9	76.49	0.38	0.36
m-CPPD	P1	−9.70	−8.66	82.6	59.55	0.34	0.70
	P2	−5.90	−6.44	72.5	97.70	0.41	0.24
m-CPPD	P1	−5.90	−7.42	72.5	61.59	0.41	0.60
Rel H	P2	−9.70	−7.80	82.6	96.17	0.34	0.18
t-CPPD	P1	−5.94	−5.22	76.6	79.95	0.56	0.57
Rel H	P2	−4.97	−4.58	75.6	79.28	0.27	0.26
m-CPPT β	P1	−9.31	−15.80	84.5	85.16	0.21	0.11
Rel H	P2	−7.33	−6.90	71.6	78.50	0.41	0.54
m-CPPM	P1	−11.27	−3.4	64.0	68.78	0.80	0.70
	P2	−7.34	−0.2	85.7	93.66	0.48	0.56
a-CPP	P	−6.7		78.2		0.80	

ACCEPTED MANUSCRIPT

Table 2: Experimental and calculated ^{43}Ca chemical shift and quadrupolar parameters for α-$Ca_2P_2O_7$, m-CPPD, t-CPPD, m-CPPT β and m-CPPM. The definitions of C_Q and η_Q are given in the experimental section. In the case of m-CPPD, results obtained before and after relaxation of the proton positions (Rel H) are presented. The spectra from which the experimental values were determined are shown in Figure S5, together with their simulation. Errors were estimated to ~2-3 ppm on δ_{iso} and ~ 0.2-0.4 MHz on C_Q, except for the m-CPPM phase for which the fitting was performed at only one magnetic field (thus leading to larger errors).

		δ_{iso} (ppm)		C_Q (MHz)		η_Q	
		Exp	Calc	Exp	Calc*	Exp	Calc
α-$Ca_2P_2O_7$[a]	Ca1	−18.0	−22.1	2.5[b]	1.84	[b]	0.61
	Ca2	12.0	6.4	2.8[b]	−2.13	[b]	0.51
m-CPPD	Ca1	14.0	12.5	1.9	2.12	0.6	0.93
	Ca2	29.0	18.0	2.0	0.85	0.6	0.74
m-CPPD	Ca1	14.0	14.9	1.9	1.96	0.6	0.96
Rel H	Ca2	29.0	17.6	2.0	−0.84	0.6	0.99
t-CPPD	Ca1	14.5	13.8	3.4	−3.11	0.3	0.42
Rel H	Ca2	12.0	12.0	2.7	−2.47	0.5	0.14
m-CPPT β	Ca1	11.0	11.9	1.8	1.57	0.6	0.43
Rel H	Ca2	7.5	11.4	2.1	2.36	0.6	0.67
m-CPPM	Ca1	33.0	15.2	2.6	−1.42	0.7	0.38
Rel tot	Ca2	20.0	5.3	4.5	−3.64	0.4	0.55

[a] For α-$Ca_2P_2O_7$, the calculated values reported here differ from those previously published,[29] due to the difference in computational code used (PARATEC *vs* Quantum Espresso).

[b] For α-$Ca_2P_2O_7$, only the quadrupolar parameter P_Q had been reported. [29]

* the sign of C_Q cannot be determined by solid state NMR experiments at room temperature.

ACCEPTED MANUSCRIPT

[1] Richette P, Bardin T, Doherty M. An update of the epidemiology of calcium pyrophosphate dihydrate crystal deposition disease. Rheumatology 2009;48:711-5.

[2] Macmullan P, McCarthy G. Treatment and management of pseudogout: insights for the clinician. Ther Adv Musculoskelet Dis 2012;4:121-31.

[3] Ea HK, Lioté F. Diagnosis and clinical manifestations of calcium pyrophosphate and basic calcium phosphate crystal deposition diseases. Rheum Dis Clin North Am 2014;40:207-29.

[4] Liu YZ, Jackson AP, Cosgrove SD. Contribution of calcium-containing crystals to cartilage degradation and synovial inflammation in osteoarthritis. Osteoarthr Cartil 2009;17:1333–40.

[5] Mandel NS. The crystal structure of calcium pyrophosphate dihydrate. Acta Crystallogr 1975; B31: 1730–34.

[6] Brown EH, Lehr JR, Smith JP, Frazier AW. Fertilizer materials, preparation and characterization of some calcium pyrophosphates. Agric Food Chem 1963;11: 214–22.

[7] Gras P. Etude Physico-chimique et structurale de pyrophosphates de calcium hydratés : application aux microcalcifications associées à l'arthrose. PhD thesis, Institut National Polytechnique de Toulouse, France, 2014

[8] Balic-Zunic T, Christoffersen MR, Christoffersen J. Structure of the β form of calcium pyrophosphate tetrahydrate. Acta Crystallogr 2000; B56:953-8.

[9] Davis NL, Mandel GS, Mandel NS, Dickerson RE. Structure of monoclinic calcium pyrophosphate tetrahydrate. J Crystallogr Spectr Res 1985; 15:513-21.

[10] Gras P, Rey C, Marsan O, Sarda S, Combes C, Synthesis and characterisation of hydrated calcium pyrophosphate phases of biological interest. Eur J Inorg Chem 2013;5886.

[11] Gras P, Teychené S, Rey C, Charvillat C, Biscans B, Sarda S, Combes C. Crystallisation of a highly metastable hydrated calcium pyrophosphate phase. CrystEngComm 2013;15:2294-300.

[12] Gras P, Ratel-Ramond N, Teychéné S, Rey C, Elkaim E, Biscans B, Sarda S, Combes C. Structure of the calcium pyrophosphate monohydrate phase ($Ca_2P_2O_7 \cdot H_2O$): towards understanding the dehydration process in calcium pyrophosphate hydrates. Acta Crystallogr 2014;C70:862-66.

[13] Slater C, Laurencin D, Burnell V, Smith ME, Grover LM, Hriljac JA, Wright AJ. Enhanced stability and local structure in biologically relevant amorphous materials containing pyrophosphate. J Mater Chem 2011; 21:18783-91.

[14] Mandel NS. The structural basis of crystal-induced membranolysis. Arthritis Rheum 1976;19:439-45.

[15] Roch-Arveiller M, Legros R, Chanaud B, Muntaner O, Strzalko S, Thuret A, Willoughby DA, Giroud JP. Inflammatory reactions induced by various calcium pyrophosphate crystals. Biomed & Phamacother 1990; 44:467-74.

[16] Swan A, Heywood B, Chapman B, Seward H, Dieppe P. Evidence for a causal relationship between the structure, size, and load of calcium pyrophosphate dehydrate crystals, and attacks of pseudogout. Ann Rheum Dis 1995; 54:825-30.

[17] Wierzbicki A, Dalal P, Madura JD, Cheung HS. Molecular dynamics simulation of crystal-induced membranolysis. J Phys Chem 2003; 107: 12346-51.

[18] Bonhomme C, Gervais C, Laurencin D. Recent NMR developments applied to organic-inorganic materials. Prog Nucl Magn Reson Spect 2014; 77:1-48.

[19] Fayon F, Duée C, Poumeyrol T, Allix M, Massiot D. Evidence of nanometric-sized phosphate clusters in bioactive glasses as revealed by sold state ^{31}P NMR. J Phys Chem C 2013; 117: 2283-8.

ACCEPTED MANUSCRIPT

[20] Pourpoint F, Gervais C, Bonhomme-Coury L, Azaïs T, Coelho C, Mauri F, Alonso B, Babonneau F, Bonhomme C. Calcium phosphates and hydroxyapatite: solid-state NMR experiments and first-principles calculations. Appl Magn Reson 2007; 32: 435-57.

[21] Pourpoint F, Coelho Diogo C, Gervais C, Bonhomme C, Fayon F, Laurencin Dalicieux S, Gennero I, Salles J-P, Howes AP, Dupree R, Hanna JV, Smith ME, Mauri F, Guerrero G, Mutin PH, Laurencin D. High-resolution solid state NMR experiments for the characterization of calcium phosphate biomaterials and biominerals. J Mater Res 2011;26:2355-68.

[22] Laurencin D, Almora-Barrios N, de Leeuw NH, Gervais C, Bonhomme C, Mauri F, Chrzanowski W, Knowles JC, Newport RJ, Wong A, Gan Z, Smith ME. Magnesium incorporation into hydroxyapatite. Biomaterials 2011;32:1826-37.

[23] Schnitzler V, Fayon F, Despas C, Khairoun I, Mellier C, Rouillon T, Massiot D, Walcarius A, Janvier P, Gauthier O, Montayon G, Bouler J-M, Bujoli B. Investigation of alendronate-doped apatitic cements as a potential technology for the prevention of osteoporotic hip fractures: critical influence of the drug introduction mode on the *in vitro* cement properties. Acta Biomater 2011;7:759-70.

[24] Despas C, Schnitzler V, Janvier P, Fayon F, Massiot D, Bouler J-M, Bujoli B, Walcarius A. High-frequency impedance measurement as a relevant tool for monitoring the apatitic cement setting reaction. Acta Biomater 2014; 10:940-50.

[25] Mellier C, Fayon F, Schnitzler V, Deniard P, Allix M, Quillard S, Massiot D, Bouler J-M, Bujoli B, Janvier P. Characterization and properties of novel gallium-doped calcium phosphate ceramics. Inorg Chem 2011; 50: 8252-60.

[26] Roiland C, Fayon F, Simon P, Massiot D. Characterization of the disordered phosphate network in $CaO-P_2O_5$ glasses by ^{31}P solid state NMR and Raman spectroscopies. J Non Cryst Solids 2011;357:1636-46.

[27] Roiland C, PhD Dissertation, Etude de l'ordre local dans les phosphates désordonnés modèles par spectroscopies RMN et Raman, Orléans University, 2007.

[28] Legrand AP, Sfihi H, Lequeux N, Lamaître J. ^{31}P solid state NMR study of the chemical setting process of a dual-paste injectable brushite cement. J Biomed Mater Res B: Appl Biomater 2009; 91:46-54.

[29] Gervais C, Laurencin D, Wong A, Pourpoint F, Labram J, Woodward B, Howes AP, Pike KJ, Dupree R, Mauri F, Bonhomme C, Smith ME. New perspectives on calcium environments in inorganic materials containing calcium-oxygen bonds: a combined computational-experimental ^{43}Ca NMR approach. Chem Phys Lett 2008; 464:42-8.

[30] Laurencin D, Smith ME. Development of ^{43}Ca solid state NMR spectroscopy as a probe of local structure in inorganic and molecular materials. Prog Nucl Magn Reson Spect 2013;68:1-40.

[31] Bryce DL. Calcium binding environments probed by ^{43}Ca NMR spectroscopy. Dalton Trans 2010;39; 8593–602.

[32] van Eck, Smith MES. Recent advances in experimental solid state NMR methodology for half-integer spin quadrupolar nuclei. Prog Nucl Magn Reson Spectrosc 1999;34:159-201.

[33] MacKenzie KJD, Smith MES. *Multinuclear Solid State NMR of Inorganic Materials*, Pergamon, 2002.

[34] Reinholdt M, Croissant J, Di Carlo L, Granier D, Gaveau P, Begu S, Devoisselle J-M, Mutin PH, Smith ME, Bonhomme C, van der Lee A, Laurencin D. Synthesis and characterization of crystalline structures based on phenylboronate ligands bound to alkaline earth cations. Inorg Chem 2011;50: 7802-10.

[35] Colas H, Bonhomme-Coury L, Coelho Diogo C, Tielens F, Babonneau F, Gervais C, Bazin D, Laurencin D, Smith ME, Hanna JV, Daudon M, Bonhomme C Whewellite, $CaC_2O_4.H_2O$: structural study by a combined NMR, crystallography and modeling approach. Cryst Eng Comm 2013;15:8840-7.

[36] Sene S, Bouchevreau B, Martineau C, Gervais C, Bonhomme C, Gaveau P, Mauri F, Bégu S, Mutin PH, Smith ME, Laurencin D. Structural study of calcium phosphonates: a combined synchrotron synchrotron powder diffraction, solid-state NMR and first-principles calculations approach. Cryst Eng Comm 2013;15:8763-75.

[37] Charpentier T. The PAW/GIPAW approach for computing NMR parameters: a new dimension added to NMR study of solids. Solid State Nucl Magn Reson 201;40:1-20.

[38] Bonhomme C, Gervais C, Babonneau F, Coelho C, Pourpoint F, Azaïs T, Ashbrook SE, Griffin JM, Yates JR, Mauri F, Pickard CJ. First-principles calculation of NMR parameters using the gauge including projector augmented wave method: a chemist's point of view. Chem. Rev. 2012;112: 5733-79.

ACCEPTED MANUSCRIPT

[39] Grover LM, Wright AJ, Gbureck U, Bolarinwa A, Song J, Liu Y, Farrar DF, Howling G, Rose J, Barralet JE. Biomaterials 2013;34,6631-37.

[40] Fung BM, Khitrin AK, Ermolaev K. An improved broadband decoupling sequence for liquid crystals and solids. J Magn Reson 2000;142:97-101.

[41] Lejeune C, Coelho C, Bonhomme-Coury L, Azaïs T, Maquet J, Bonhomme C. Studies of silicophosphate derivatives by $^{31}P \rightarrow {}^{29}Si$ CP MAS NMR. Solid State NMR 2005;27:242-46.

[42] Kentgens APM, Verhagen R. Advantages of double frequency sweeps in static, MAS and MQMAS NMR of spins I = 3/2 nuclei. Chem Phys Lett 1999;300:435-43.

[43] Iuga D, Schafer H, Verhagen R, Kentgens APM. Population and coherence transfer induced by double frequency sweeps in half-integer quadrupolar spin systems. J Magn Reson 2000;147:192-209.

[44] Yao HT, Kwak D, Sakellariou D, Emsley L, Grandinetti PJ. Sensitivity enhancement of the central transition NMR signal of quadrupolar nuclei under magic-angle spinning. Chem Phys Lett 2000;327:85-90.

[45] Lesage A. Recent advances in solid-state NMR spectroscopy of spins I = ½ nuclei. Phys Chem Chem Phys 2009;11: 6876-91.

[46] Sakellariou D, Lesage A, Hodgkinson P, Emsley L. Homonuclear dipolar decoupling in solid-state NMR using continuous phase modulation. Chem Phys Lett 2000;319:253-60.

[47] Lesage A, Sakellariou D, Hediger S, Elena B, Charmont P, Steuernagel S, Emsley L. Experimental aspects of proton NMR spectroscopy in solids using phase-modulated homonuclear dipolar decoupling. J Magn Reson 2003;163:105-13.

[48] Pickard C. J., Mauri F. All-electron magnetic response with pseudopotentials: NMR chemical shifts. Phys Rev B 2001;63: 245101.

[49] Giannozzi P, Baroni S, Bonini N, Calandra M, Car R, Cavazzoni C, Ceresoli D, Chiarotti G L, Cococcioni M, Dabo I, Dal Corso A, de Gironcoli S, Fabris S, Fratesi G, Gebauer R, Gerstmann U, Gougoussis C, Kokalj A, Lazzeri M, Martin-Samos L, Marzari N, Mauri F, Mazzarello R, Paolini S, Pasquarello A, Paulatto L, Sbraccia C, Scandolo S, Sclauzero G, Seitsonen AP, Smogunov A, Umari P, Wentzcovitch RM. QUANTUM ESPRESSO: a modular and open-source software project for quantum simulations of materials. J Phys Condensed Matter: an Institute of Physics journal 2009;21:395502.

[50] For t-CPPD: see ICSD_1912.

[51] For m-CPPT : see ICSD_280410.

[52] Kresse G, Hafner J. Ab-initio molecular-dynamics for liquid-metals. Phys Rev B 1993;47:558–61.

[53] For α-$Ca_2P_2O_7$: see ICSD_ 22225.

[54] Perdew JP, Burke K, Ernzerhof M. Generalized Gradient Approximation Made Simple. Phys Rev Lett 1996;77: 3865-68.

[55] Troullier N, Martins JL. Efficient pseudopotentials for plane-wave calculations. Phys Rev B 1991;43:1993-2006.

[56] Kleinman L, Bylander D. Efficacious form for model pseudopotentials. Phys Rev Lett 1982;48:1425.

[57] Burgess K M N, Xu Y,Leclerc M C, Bryce D L. Alkaline-Earth Metal Carboxylates Characterized by ^{43}Ca and ^{87}Sr Solid-State NMR: Impact of Metal-Amine Bonding. Inorg Chem 2014 ;53,552–61.

[58] Wyckoff RWG. *Crystals Structures*, vol. 3., Wiley:NewYork, 2nd ed.,1963;31.

[59] Xue X. Determination of J coupling constants between spin-1/2 and quadrupolar nuclei in inorganic solids from spin echo and refocused INEPT experiments: a case study on $AlPO_4$ berlinite. Solid State NMR 2010;38:62-73.

ACCEPTED MANUSCRIPT

[60] Stievano L,Tielens F, Lopes I, Folliet N, Gervais C, Costa D, Lambert J-F. Density functional theory modeling and calculation of NMR parameters: an ab initio study of the polymorphs of bulk glycine. Cryst Growth Design 2010;10:3657-67.

[61] Florian P, Fayon F, Massiot D. $^{2}J_{Si\text{-}O\text{-}Si}$ scalar spin-spin coupling in the solid state: crystalline and glassy wollastonite $CaSiO_3$. J Phys Chem C 2009;113: 2562-72.

[62] Massiot D, Fayon F, Capron M, King I, Le Calvé S, Alonso B, Durand J-O, Bujoli B, Gan Z, Hoatson G. Modelling one-and two-dimensional solid-state NMR spectra. Magn Reson Chem 2002;20:70-6.

[63] Bonhomme C, Gervais C, Coelho C, Pourpoint F, Azaïs T, Bonhomme-Coury L, Babonneau F, Jacob G, Ferrari M, Canet D, Yates JR, Pickard CJ, Joyce SA, Mauri F, Massiot D. New perspectives in the PAW/GIPAW approach: $J_{P\text{-}O\text{-}Si}$ coupling constants, antisymmetric parts of shift tensors and NQR predictions. Magn Reson Chem 2010;48, suppl 1:S86-102.

[64] Gervais C, Coelho C, Azaïs T, Maquet J, Laurent G, Pourpoint F, Bonhomme C, Florian P, Alonso P, Guerrero G, Mutin PH, Mauri F. First principles calculations of phenylphosphinic acid $C_6H_4HPO(OH)$: assignments, orientations of tensors by local field experiments and effect of molecular motion. J Magn Reson 2007;187:131-40.

[65] Lazarev AN, *Vibrational Spectra and Structure of Silicates*, translated from the Russian by GD Archard. Consultants Bureau, New York, 1972.

[66] Cruickshank DWJ. The role of 3d-orbitals in π-bonds between (a) silicon, phosphorus, sulphur, or chlorine and (b) oxygen or nitrogen. J Chem Soc 1961:5486-504.

[67] Rulmont A, Cahay R, Liegeois-Duyckaerts M, Tarte P. Vibrational spectroscopy of phosphate: Some general correlations between structure and spectra. Eur J Solid State Inorg Chem 1991;28: 207–19.

[68] Balic Zunic T, Vickovic I. IVTON – a program for the calculation of geometrical aspects of crystal structures and some crystal chemical applications. J Appl Cryst 1996;29:305-6.

[69] Gambuzzi E, Pedone A, Menziani MC, Angeli F, Florian P, Charpentier T. Calcium environment in silicate and aluminosilicate glasses probed by 43Ca MQMAS NMR experiments and MD-GIPAW calculations. Solid State Nucl Magn Reson 2015.68-69;31-6.

[70] Jones A C, Chuck A J, Arie E A, Green D J, Doherty M. Diseases associated with Calcium Pyrophosphate Deposition disease. Semin. Arthristis Rheum. 1992; 22: 188–202.

[71] McClure J, Smith P S. Calcium pyrophosphate dihydrate deposition in the intervertebral discs in a case of Wilson's disease. J. Clin. Pathol. 1983; 36: 764–768.

[72] Wright G D, Doherty M. Calcium pyrophosphate crystal deposition is not always ‘ wear and tear ’ or aging. Ann. Rheum. Dis. 1997; 56: 586–588.

ACCEPTED MANUSCRIPT

Calcium Pyrophosphates (CPP)

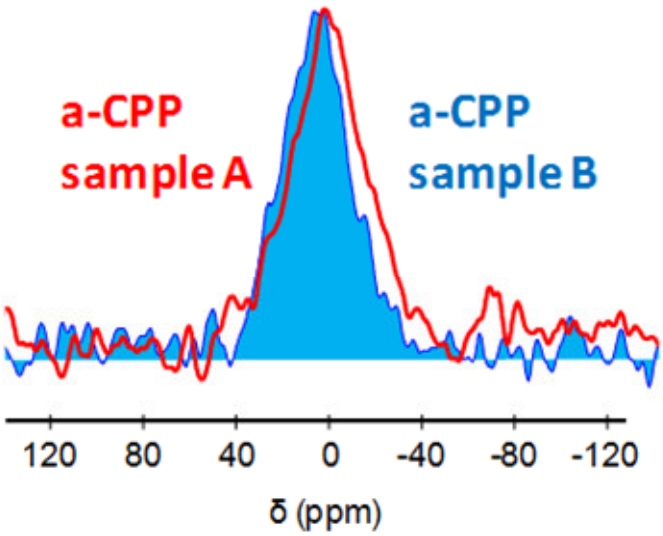

ACCEPTED MANUSCRIPT